Progress In Electromagnetics Research M, Vol. 84, 21–30, 2019

Estimating Electric Parameters of Nonhomogeneous Laminar Materials Using Differo-Integral Method

Adam Steckiewicz* **and Boguslaw Butrylo**

Abstract—The electrical network model and differo-integral method (D-IM) were applied to electrical parameters estimation of nonhomogeneous composite materials. The laminar composite is arranged of conductive unit cells with adjustable geometry. Modification of unit cell's internal geometry results in change of composite's effective properties. Stationary electric and magnetic fields of exemplary structures were numerically analyzed. Theoretical computations along with network model were verified by experimental measurements of 10 fabricated samples. Obtained results indicate that D-IM is a valuable tool for qualitative and quantitative estimation of electrical parameters.

1. INTRODUCTION

Artificial electromagnetic (EM) structures attract great interest nowadays. Their ability to achieve wide range of selected parameters has led to many applications. Recent advances in fields control introduced metamaterials [1, 2] operating in thermal, electric and magnetic fields. Fractal inductors [3] are an alternative for planar inductors in electronic devices, and textile composites are used for EM shielding [4], frequency selective surfaces as filtering devices [5], while metamaterials allows fabricating ideal absorbers [6]. Most of the modern EM composites are inhomogeneous materials with complex structures resulting from various shapes of fillers, which complicates the analysis of their properties [7]. Despite some analytical field distribution models in the systems with rectangular cross-section [8], numerical methods such as finite element method [9], higher order method of moments [10], and finite-difference time-domain method [11] are used to extract the effective properties of composites. However, these methods are advanced, computationally expensive, and mostly applied to the analysis of dielectric structures with spherical [9, 10] fillers in high-frequency EM fields.

The nonhomogeneous composite with conductive layer (Fig. 1(a)) can be distinguished from many artificial materials. Applications as elastic low power heaters or low-pass filters [12] have been proposed and tested numerically. Composite's effective electric and magnetic properties are adjusted at the lowest structural level, by the selection of geometrical parameters and constituent materials of the elementary unit cell Ω^e (Fig. 2(b), Fig. 3). Since the nonhomogeneous composite consists of many conductive elements Ω^e arranged periodically on the nonconductive base Ω^B, an electrical network model is proposed as a primary analysis tool for calculating electric potential distribution at material's surface as well as its equivalent impedance or power losses in large scale systems. However, a solution of the network model requires the identification of lumped parameters (resistance R_e, self inductance L_e, and coupling coefficient k of elements Ω^e).

In this article, a numerical differo-integral method (D-IM) for evaluating two-dimensional (2D) local stationary electric and magnetic field distributions and lumped parameters of the unit cell is presented. Proposed composite materials are designed to operate in low and medium-frequency fields ($f < 1\,\mathrm{MHz}$). Unit cell's characteristic size is much smaller than wavelength ($d_e \ll \lambda$), hence quasi-static approach

Received 2 June 2019, Accepted 31 July 2019, Scheduled 16 August 2019
* Corresponding author: Adam Steckiewicz (a.steckiewicz@pb.edu.pl).
The authors are with the Faculty of Electrical Engineering, Bialystok University of Technology, 15-351 Bialystok, Poland.

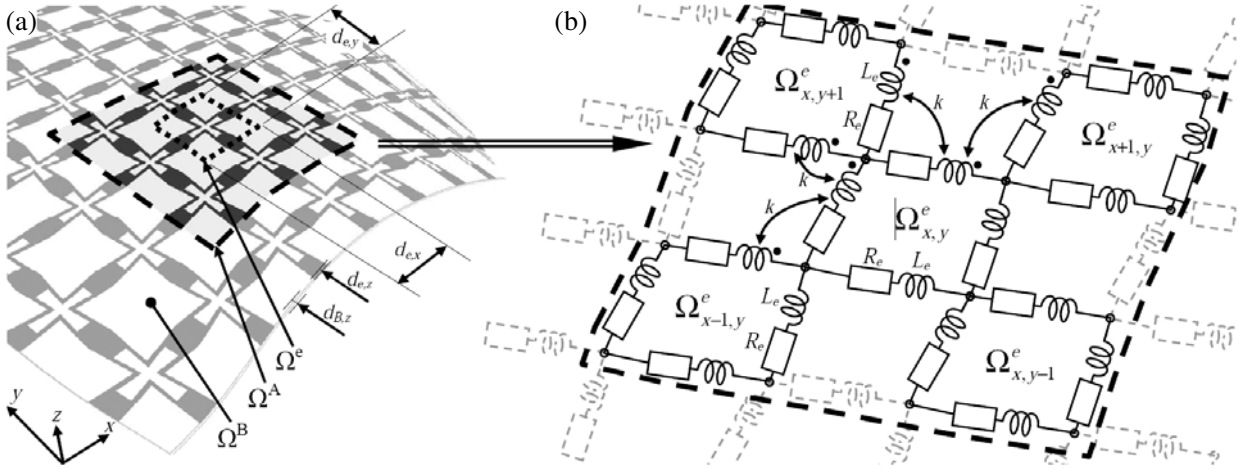

Figure 1. Exemplary composite structure: (a) view on the composite with periodically arranged conductive elements Ω^e on the dielectric base Ω^B; (b) electrical network model of the composite with elementary resistance R_e, inductance L_e and coupling coefficient k.

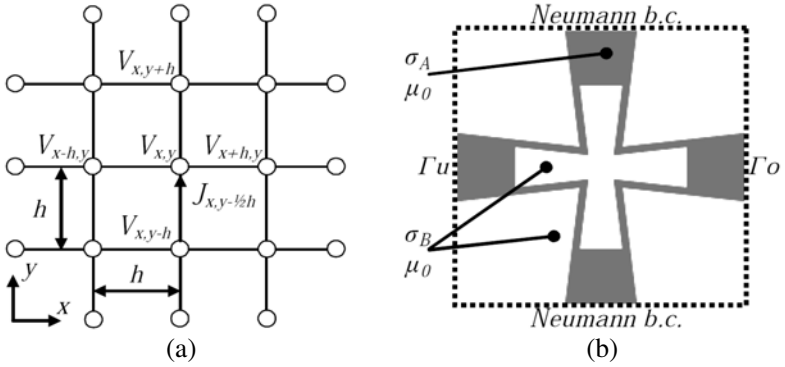

Figure 2. Numerical model of the unit cell: (a) uniform mesh for the finite difference algorithm; (b) 2D representation of Ω^e.

for local field distribution calculation may be applied. Combination of the finite difference method and integral vector potential formulation for thin-film structures simplifies quasi-static EM field analysis. Lumped parameters estimated by D-IM as well as proposed network model are verified by experimental measurements which indicate acceptable qualitative and quantitative agreement.

2. PROBLEM FORMULATION

2.1. Electrical Network Model

Nonhomogeneous laminar composite consists of at least two phases: the functional layer Ω^A arranged with connected unit cells Ω^e and elastic adhesive base Ω^B (Fig. 1). In low-frequency ($f < 1\,\mathrm{MHz}$) EM fields, where external and induced currents flow through Ω^A layer, any displacement currents are negligible. Thus dielectric, nonconductive base Ω^B is omitted. Despite this assumption, numerical EM field analysis becomes disadvantageous by requiring a lot of computational effort when large scale systems with hundreds or thousands cells are considered.

Electrical network model of the composite focuses on its periodic functional phase. Each unit cell Ω^e is represented as a parallel-series connection of four identical elementary resistances R_e and inductances L_e (Fig. 1(b)). Individual branch consisting of a series connection of R_e and L_e represents one quarter of Ω^e structure. Since the size and period of Ω^e are relatively small (several millimeters),

coupling coefficient k is introduced to consider energy transfer via magnetic field. For simplification it is assumed that the magnetic coupling occurs only between neighboring cells.

2.2. Electric Field Analysis

Any analysis of composite (network model) requires prior identification of the unit cell's lumped parameters. For this task the differential algorithm is applied. Let us consider the stationary field of electric potentials $V(x,y)$ assigned to vertexes of 2D mesh with spacing h in x and y directions (Fig. 2(a)). Components of current density vector $\mathbf{J}(x,y)$ are located at the orthogonal edges. The differential form of Ohm's law defines the relationship among $V(x,y)$, $\mathbf{J}(x,y)$, and $\sigma(x,y)$

$$\mathbf{J}(x,y) = -\sigma(x,y)\nabla V(x,y) = -\sigma(x,y)\left[\begin{array}{cc} \frac{\partial}{\partial x} & \frac{\partial}{\partial y} \end{array}\right] V(x,y). \tag{1}$$

The discretization of Eq. (1) on a square mesh and the approximation of the derivatives by the linear Euler's scheme (as an example vector element $J_{x,y-1/2h}$ will be used) results in

$$J_{x,y-1/2\,h} = -\sigma_{x,y-1/2\,h}\frac{\partial V}{\partial y}\bigg|_{x,y-1/2\,h} = -\sigma_{x,y-1/2\,h}\frac{V_{x,y} - V_{x,y-h}}{h}. \tag{2}$$

Then the transformation of Eq. (2) leads to the form

$$b^{-1}_{x,y-1/2\,h} J_{x,y-1/2\,h} + c_{x,y-1/2\,h} V_{x,y-h} + c_{x,y} V_{x,y} = 0. \tag{3}$$

where $b_{x,y-1/2h} = h^{-1}\sigma_{x,y-1/2h}$; $c_{x,y-1/2h} = -1$ ($J_{x,y-1/2h}$ directed out of vertex) and $c_{x,y} = 1$ ($J_{x,y-1/2h}$ directed into vertex) are incidence matrix elements ($c = 0$ in other cases). For each branch in mesh and both directions x and y, an equation in the form of Eq. (3) is generated, thus the system of $p = (n-1)m + n(m-1)$ equations is formed, where n and m are respectively the total number of rows and columns of the mesh. The matrix form of these equations is then specified as

$$\left[\begin{array}{cc} \mathbf{B} & \mathbf{C} \\ \mathbf{C^T} & \mathbf{0_m} \end{array}\right] \cdot \left[\begin{array}{c} \mathbf{J} \\ \mathbf{V} \end{array}\right] = \left[\begin{array}{c} \mathbf{u} \\ \mathbf{0_v} \end{array}\right]. \tag{4}$$

where $\mathbf{B} = \mathrm{diag}\left(b^{-1}_{0,0};\ b^{-1}_{h,0};\ \ldots\ ;\ b^{-1}_{n\cdot h,\, m\cdot h}\right)$, $\dim(\mathbf{B}) = p\times p$; $\mathbf{C}$ is an incidence matrix, $\dim(\mathbf{C}) = p\times n\cdot m$; $\mathbf{J}$ is a vector of unknown current densities, $\dim(\mathbf{J}) = p\times 1$; $\mathbf{V}$ is a vector of unknown electric potentials, $\dim(\mathbf{V}) = n\cdot m\times 1$; $\mathbf{u}$ is an input vector of the applied electric potentials; $\mathbf{0}_m$ and $\mathbf{0}_v$ are the null matrix and vector, respectively. Applying Woodbury's formula to Eq. (4),. one may obtain the solution for $\mathbf{J}$

$$\mathbf{J} = \mathbf{B}^{-1}\mathbf{u} - \mathbf{B}^{-1}\mathbf{C}\underbrace{\left(\mathbf{C}^T\mathbf{B}^{-1}\mathbf{C}\right)^{-1}\left(\mathbf{C}^T\mathbf{B}^{-1}\mathbf{u}\right)}_{\mathbf{x}}. \tag{5}$$

where $\mathbf{x}$ is an unknown vector. In Eq. (5), the inverse of $\mathbf{B}$ appears, although $\mathbf{B}$ is a diagonal matrix, hence its inverse is trivial. The main effort is put into computation of $\mathbf{x}$ by numeric solvers.

Differential algorithm is applied to solve the electric field of the unit cell. Each Ω^e is represented as a 2D sketch (Fig. 2(b)) with isotropic constituent materials A (conductor) and B (isolator) assigned to contrasting colors. At the top and bottom edges, the Neumann boundary conditions (b.c.) are applied. On the left Γu and right Γo edge Dirichlet b.c. are assigned where in typical case Γu is a voltage source ($V_{\Gamma u} = 1\,\mathrm{V}$), and Γo has a reference potential ($V_{\Gamma o} = 0\,\mathrm{V}$).

2.3. Magnetic Field Analysis

Electric field computations are performed for restricted 2D model (Fig. 2(b)) whose length $d_{e,x}$ and width $d_{e,y}$ are equal to external size of unit cell $d_{e,x} = d_{e,y} = d_e$. Since the unit cell is thin ($d_{e,z} \ll d_e$), magnetic field computations are significantly simplified. Let us assume that $\mathbf{J}$ is found by differential algorithm. The stationary magnetic field (magnetic vector potential $\mathbf{A}$) is computed using Helmholtz theorem of vector potential for thin-film systems

$$\mathbf{A}\,(x,y) = \frac{\mu_0}{4\pi} d_{e,z} \iint\limits_S \frac{\mathbf{J}\,(x',y')}{\sqrt{(x-x')^2 + (y-y')^2}} dS. \tag{6}$$

where S-2D model surface of a size $d_{e,x} \times d_{e,y}$ in [m^2]; μ_0 — magnetic permeability of air in [H/m], (x, y) — observation point coordinates, (x', y') — source point coordinates. Since the differential mesh is used the numerical form of Eq. (6), for longitudinal and perpendicular components of $\mathbf{A}$, will be presented in form

$$A_{x-1/2\ \mathrm{h},y} = \frac{\mu_0}{4\pi} d_{e,z} \sum_{i=1}^{n} \sum_{j=1}^{m} \frac{J_{i\cdot h-1/2\ \mathrm{h},j\cdot h}}{\sqrt{(x - i\cdot h)^2 + (y - j\cdot h)^2}}, \tag{7a}$$

$$A_{x,y-1/2\ h} = \frac{\mu_0}{4\pi} d_{e,z} \sum_{i=1}^{n} \sum_{j=1}^{m} \frac{J_{i\cdot h,j\cdot h-1/2\ \mathrm{h}}}{\sqrt{(x - i\cdot h)^2 + (y - j\cdot h)^2}}, \tag{7b}$$

where i is a row number, and j is a column number of differential mesh (Fig. 2(a)).

If constituent materials and infinite space around the unit cell are nonmagnetic, the numerical integration of Eqs. (7a) and (7b) permits calculation of the magnetic field in the cross section of Ω^e. The magnetic field is directly calculated for only restricted 2D model with natural Neumann boundary conditions at the unit cell's external edges, and no additional b.c. are required.

2.4. Lumped Parameters

Differential approximation of electric field and integral magnetic field calculations are applied to the quasi-static field analysis, and combined together, they form the differo-integral method (D-IM). Calculated field distributions of the analyzed unit cell are used for lumped parameters estimation. Firstly, a total current is calculated

$$I = d_{e,z} \int_{\Gamma u} |\mathbf{J}|\, dy, \tag{8}$$

and then elementary resistance is given as

$$R_e = \frac{V_{\Gamma u} - V_{\Gamma o}}{I}. \tag{9}$$

Secondly, the definitions of the total magnetic energy

$$W = \frac{1}{2} d_{e,z} \iint_S (\mathbf{A}\cdot\mathbf{J})\, dS, \tag{10a}$$

$$W = \frac{1}{2} L_e I^2, \tag{10b}$$

are combined altogether with Eq. (8), and as a result the formula for self-inductance is obtained

$$L_e = \frac{d_{e,z} \iint_S (\mathbf{A}\cdot\mathbf{J})\, dS}{I^2}. \tag{11}$$

While Equation (9) is easily found, Equation (11) requires another numerical integration over model's surface. However, this integral has non-zero values only for conductive parts where $\mathbf{J} \neq 0$. This emphasizes two advantages of D-IM:

- solution for only conductive parts is required;
- electric and magnetic fields are found in 2D model (cross section) of the unit cell.

In order to estimate coupling coefficient k, it is sufficient to find self inductance L_e of a single unit cell, then enhance model to a series connection of two adjacent unit cells and compute total inductance L_t. Finally, coupling coefficient may be calculated as

$$k = \frac{L_t}{2L_e} - 1. \tag{12}$$

Equations (9), (11), and (12) express all necessary parameters of the proposed equivalent circuit model (Fig. 1(b)). For the periodically arranged composite structure, they have to be calculated once, since all of the unit cells are identical.

2.5. Homogenization Procedure

Calculated lumped parameters may be utilized to extract the effective electrical conductivity and permeability of the composite. Comparing the unit cell with an equivalent, homogenous, rectangular conductor possessing identical resistance

$$R_e = \frac{d_{e,x}}{\sigma_{eff} d_{e,y} d_{e,z}} \tag{13}$$

and assuming $d_{e,x} = d_{e,y} = d_e$, Equation (13) will be transformed into

$$\sigma_{eff} = (R_e d_{e,z})^{-1}. \tag{14}$$

Similarly, comparing inductance of the unit cell with inductance of a rectangular conductor, the effective relative permeability will be defined as

$$\mu_{eff} = \frac{L_e - L_1}{a_L} + 1, \tag{15}$$

where L_1 is the inductance of a rectangular conductor for $\mu_{eff} = \mu_1 = 1$

$$L_1 = \frac{\mu_0}{2\pi} d_e \left[\ln\left(\frac{2d_e}{d_e + d_{e,z}}\right) - 0.2235 \ln\left(\frac{d_e + d_{e,z}}{d_e}\right) + 0.5 \right]. \tag{16}$$

The linear approximation coefficient a_L

$$a_L = \frac{L_1 - L_a}{\mu_1 - \mu_a}, \tag{17}$$

describes the relation between homogeneous rectangular conductor self-inductance and its relative permeability. Theoretical prediction of its value may be performed by a numerical calculation of a magnetic field distribution in a homogeneous slab possessing designed external length ($d_{e,x}$), width ($d_{e,y}$), and height ($d_{e,z}$), as well as some relative permeability ($\mu_a > 1$), in order to retrieve corresponding inductance L_a. Combining Eqs. (16) and (17) with Eq. (15), one will find effective relative permeability of the composite for non-stationary magnetic fields.

3. EXPERIMENTAL SETUP

3.1. Analyzed Structure

For the purpose of testing the presented D-IM two isotropic geometries of the unit cell are proposed. In relation to homogeneous conductive plate, *star* structure (Fig. 3(a)) is ideal to obtain higher values of both resistance and inductance by the adjustment of internal geometrical parameters. d_1 and d_2 modify the location of *star*'s edge (conducting path) which changes electric connection (d_1) and path's rotation

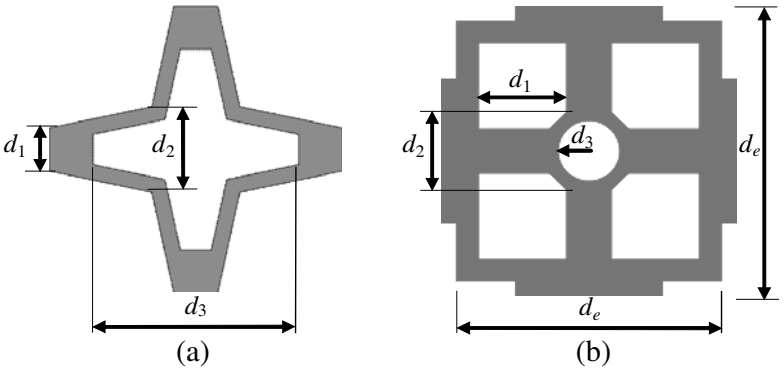

Figure 3. Structure and geometrical parameters of the unit cell Ω^e: (a) *star* element; (b) *lattice* element.

(d_2), while d_3 regulates the internal resection. *Lattice* structure (Fig. 3(b)) has three parallel conducting paths. Its inductance is slightly higher then homogeneous plate and remain similar despite the values of geometrical parameters, while resistance changes significantly. For example, square resections are modified by d_1, circular resection by d_3, and central conducting area diameter by d_2.

Considered structures have identical external size $d_e = 10\,\text{mm}$ and thickness $d_{e,z} = 0.035\,\text{mm}$, which satisfies the condition $d_{e,z} \ll d_e$. The constituent material A is a copper ($\sigma_A = 5.7 \cdot 10^7\,\text{S/m}$), and material B is a ceramic-filled PTFE ($\sigma_B \approx 0\,\text{S/m}$). Presented unit cells are firstly calculated by D-IM (22500 degrees of freedom) and then fabricated using identical materials.

3.2. Equivalent Circuit

Constituent material (copper) and size (10 mm) of Ω^e are directly connected with values of its lumped parameters which are expected to be relatively small (milliohms and microinductances). Experimental estimation of R_e, L_e, and k requires preparation of a sample consisting of many serially connected unit cells. Hence, 10 samples (5 *star* and 5 *lattice* structures) with 20 linearly arranged unit cells are analyzed and fabricated (Fig. 4(a)). The network model of an equivalent complex system (Fig. 5(a)) is reduced to simpler one (Fig. 5(b)), which is a chain circuit composed of identical lumped parameters and positive magnetic coupling between neighboring elements. This series connection leads to total resistance $R_t = 20R_e$ and inductance $L_t = 20L_e + 38kL_e$ of a single sample (Fig. 5(c)).

The geometries of samples are chosen in a way to obtain high structural variety. Lumped parameters R_t and L_t are measured on an experimental stand using Hameg HM8118LCR Bridge with 4-wire Kelvin probes (Fig. 4(b)). The Kelvin clips and samples are placed in a 3D printed measuring stand with

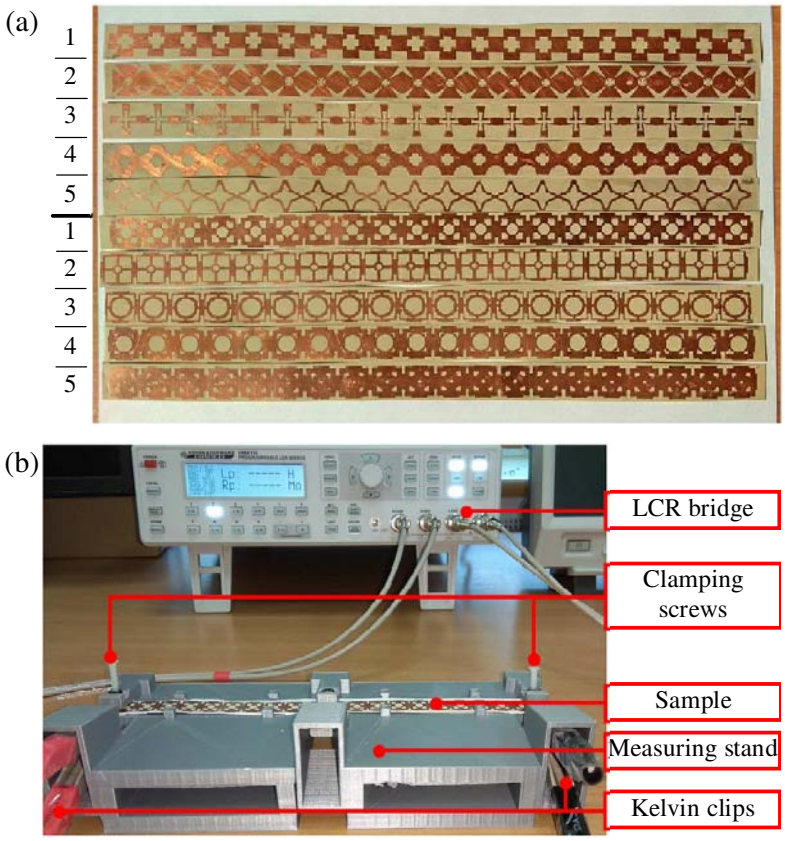

Figure 4. Experimental stand: (a) photograph of 10 fabricated samples (5 *star* and 5 *lattice*, 20 cells each); (b) LCR bridge and 3D printed measuring stand with insulating clamping screws and grips for samples and clips positioning.

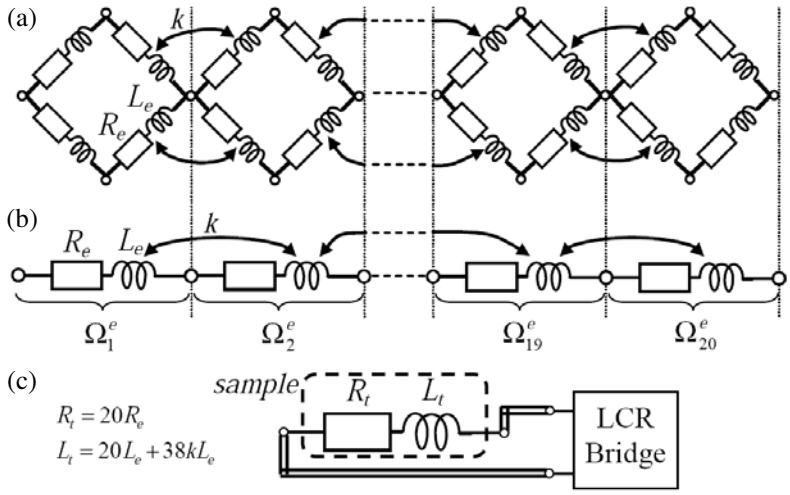

Figure 5. Electrical model of tested samples: (a) full circuit model; (b) simplified circuit; (c) measured impedance of a sample with series resistance R_t and coupled inductance L_t.

insulating clamping screws for the reduction of parasitic impedances. In every test, each sample is measured at three source voltage frequencies: 5, 10, and 20 kHz. Then the obtained results are averaged. The mean accuracy of all measurements is $\pm 0.54\%$.

4. RESULTS AND DISCUSSION

Firstly, the surface distribution of current density and magnetic vector potential are calculated by D-IM for all the unit cells (samples). The *star* sample number 3 (Fig. 6) is a representative example. Current density norm distribution (Fig. 6(a)) shows areas with higher (thin conducting paths in a center part) and lower densities (thick connections near edges) of flowing charge. On the basis of magnetic vector potential $\mathbf{A}$, the magnetic induction $\mathbf{B} = \nabla \times \mathbf{A}$ is found (Fig. 6(b)). In the cross section of Ω^e magnetic field has only z-component, whose distribution is very heterogeneous and strongly depends on cell's structure.

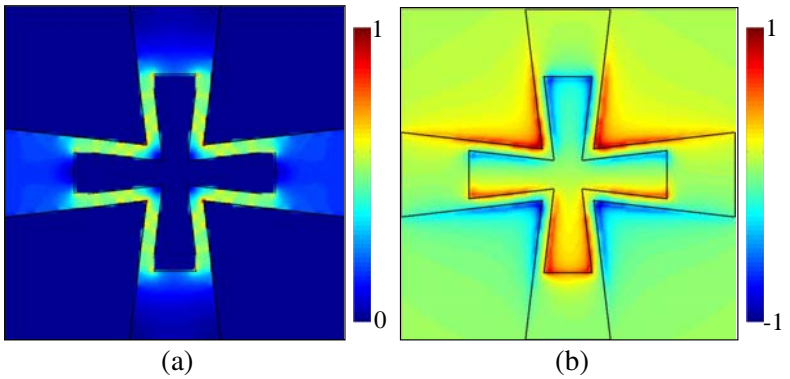

Figure 6. *Star* element No. 3 — computed by D-IM: (a) relative current density norm $|\mathbf{J}|$; (b) relative magnetic induction B_z.

Calculated total resistance of *star* structures matches acceptably with measured ones (Fig. 7) both qualitatively and quantitatively. Good qualitative agreement of the results can be seen for *lattice* samples. Obtained results also indicate an ability of precise selection and determination of resistance by simple adjustment of the unit cell's geometrical parameters.

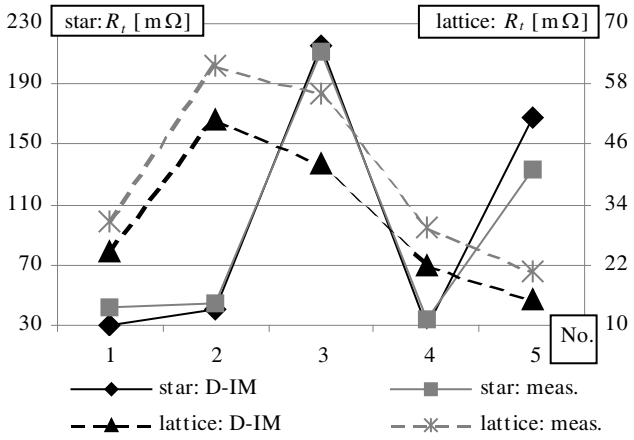

Figure 7. Calculated and measured total resistance of samples.

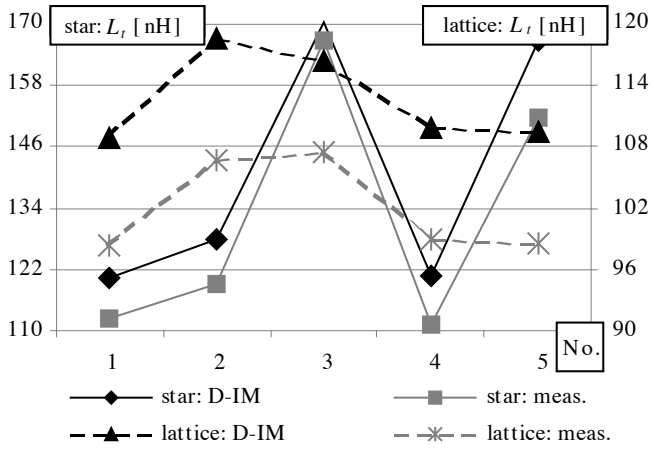

Figure 8. Calculated and measured total inductance of samples.

Similar to R_t, total inductances L_t of *star* cells were predicted accurately (Fig. 8). Most of all, qualitative agreement of theoretical and measured values is clearly seen for every sample. While change in *lattice*'s resistance is achieved with different structures, total inductance preserves similar values. Despite this, D-IM is still able to follow and model even subtle change of parameters.

Table 1. Relative difference between calculated and measured total resistance R_t and inductance L_t.

No.	*Star*		*Lattice*	
	ΔR_e	ΔL_e	ΔR_e	ΔL_e
1	−29.11%	7.11%	−18.86%	10.74%
2	−9.10%	7.37%	−17.33%	11.08%
3	1.94%	2.00%	−24.40%	8.32%
4	−18.78%	8.60%	−25.43%	11.03%
5	26.77%	10.08%	−26.45%	11.19%
Avg	−5.66%	7.03%	−22.49%	10.47%

Relative differences

$$\Delta R_e = \frac{R_{D-IM} - R_{meas.}}{R_{meas.}} 100\%. \tag{18a}$$

$$\Delta L_e = \frac{L_{D-IM} - L_{meas.}}{L_{meas.}} 100\%. \tag{18b}$$

of lumped parameters between electrical network model of the samples and their measured parameters (Table 1) confirm sufficient accuracy of D-IM. The average relative difference $\Delta L_e = 10.47\%$, while for resistance mean absolute relative error $|\Delta R_e|$ is below 23%. Hence, the unit cell's inductance is estimated with smaller relative error than resistance. One of the main reasons for this is a nonuniform surface thickness and conductivity of a copper layer used for sample's fabrication. These factors have a strong impact on the total resistance but minor impact on self inductance and coupling coefficient.

5. CONCLUSION

Nonhomogeneous composite materials are represented by complex electrical networks. Since composite operates at low frequency field, lumped parameters (resistance, self inductance, and coupling coefficient) are required. For the simplification of electric and magnetic field analysis, the numerical differo-integral algorithm is proposed and presented. For the purpose of D-IM verification, the isotropic *star* and *lattice* structures are computed numerically, and then 10 different samples are fabricated and measured. The mean relative difference between theoretical and experimental results are below 11% and 23% for magnetic and electric parameters, respectively. Thus, D-IM provides acceptable qualitative accuracy for estimating lumped electrical parameters.

ACKNOWLEDGMENT

This work was supported by the Ministry of Science and Higher Education in Poland under work No. MB/WE/5/2018.

REFERENCES

1. Han, T. and C.-W. Qiu, "Transformation Laplacian metamaterials: recent advances in manipulating thermal and DC fields," *J. Opt.*, Vol. 18, No. 4, 1–13, 2016.
2. Navau, C., R. Mach-Batlle, A. Parra, J. Prat-Camps, S. Laut, N. Del-Valle, and A. Sanchez, "Enhancing the sensitivity of magnetic sensors by 3D metamaterial shells," *Sci. Rep.*, Vol. 7, 1–9, 2017.
3. Djuric, S., "Koch fractal inductors printed on flexible substrate," *Electron. Lett.*, Vol. 52, No. 8, 581–583, 2016.
4. Ziaja, J., M. Jaroszewki, and M. Lewandowski, "EMI shielding using composite materials with two sources magnetron sputtering," *IOP Conf. Ser.: Mater. Sci. and Eng.*, Vol. 113, No. 1, 012010, 2016.
5. Taghizadeh, M., M. Maddahali, and R. Abed, "Novel band-pass frequency selective surface with stable response," *8th Int. Symp. on Telecommun. (IST'2016)*, 428–431, Tehran, Iran, September 2016.
6. Xu, G., J. Zhang, X. Zang, O. Sugihara, H. Zhao, and B. Cai, "0.1–20 THz ultra-broadband perfect absorber via a flat multi-layer structure," *Opt. Express*, Vol. 24, No. 20, 2016.
7. Moore, R., *Electromagnetic Composites Handbook*, Ch. 5, McGraw-Hill Education, 2016.
8. Zareba, M., "Application of Duhamel's theorem in the analysis of the thermal field of a rectangular busbar," *J. of Electr. Eng. and Technol.*, Vol. 14, No. 1, 2019.
9. Zhong, S.-L. and Z.-M. Dang, "Prediction on effective permittivity of 0-3 connectivity particle/polymer composites at low concentration with finite element method," *IEEE Tran. on Dielectr. and Electr. Insul.*, Vol. 25, No. 6, 2018.

10. Lin, Z., X. Zhao, Y. Zhang, and H. Liu, "Higher order method of moments analysis of metallic waveguides loaded with composite metallic and dielectric structures," *IEEE Tran. on Antennas And Propag.*, Vol. 66, No. 9, 2018.
11. Choroszucho, A., "Analysis of the influence of the complex structure of clay hollow bricks on the values of electric field intensity by using the FDTD method," *Arch. of Electr. Eng.*, Vol. 65, No. 4, 2016.
12. Steckiewicz, A. and B. Butrylo, "An application of PSO algorithm for multi-criteria geometry optimization of printed low-pass filters based on conductive periodic structures," *Proc. of SPIE Conf. on Photonics Appl. in Astron., Commun., Ind., and High Energy Phys. Exp.*, Wilga, Poland, May–June 2017.